Conversion and manipulation of radial quantum modes in second-harmonic-generation processes

Rui-Zhi Zhao [1,2] Rong-Er Lu,[1,2] Xu-Hao Hong,[1,3] Xia Feng,[1,2] Ya-Guang Xu,[1,2] Xu-Dong Yuan,[1,2] Chao Zhang,[1,2,*]
Yi-Qiang Qin,[1,2,†] and Yong-Yuan Zhu[1,3]

[1]*National Laboratory of Solid State Microstructures and Collaborative Innovation Center of Advanced Microstructures,
Nanjing University, Nanjing 210093, China*
[2]*College of Engineering and Applied Sciences, Nanjing University, Nanjing 210093, China*
[3]*School of Physics, Nanjing University, Nanjing 210093, China*

The second-harmonic generation of Laguerre-Gaussian (LG) beams is investigated in this paper with a coupled equation set deduced from the nonlinear paraxial equations. Under the guidance of this coupled equation set, the conversion and propagation characteristics for individual LG modes in the second-harmonic (SH) generation process are studied quantitatively. Furthermore, we show that a periodic quasi-phase-matching crystal can be used as an integrated device to produce a controllable multimode SH source. By controlling the length or temperature of crystal each LG mode of the SH wave can be manipulated separately, instead of treating the SH wave as a whole. This method might be useful in mode division multiplexing system to expand the communication capacity, and thus has potential applications in optical communication.

I. INTRODUCTION

In 1992, Allen and his coworkers revealed that the phase term $\exp(il\varphi)$ in a vortex beam denoted orbital angular momentum (OAM) [1]. From then on, optical vortices have drawn more and more attention. Due to its unique and attractive optical property, the optical vortex is applied to many fields, such as optical manipulation [2,3], optical communications [4], and quantum information [5,6]. In recent years, some properties of vortex beams, such as dichroism [7,8] and self-torque [9] have been reported. The Laguerre-Gaussian (LG) beam is one of the most common and well-studied vortex beams. It is characterized by two quantum numbers l and $p \cdot l$ is the azimuthal quantum number representing the number of azimuthal cycles in phase profile and also regarded as the topological charge. p is the radial quantum number representing the number of intensity rings of a LG beam and also regarded as the hyperbolic momentum charge [10]. Because of the association with OAM, the azimuthal quantum number l has attracted the majority of attention. The radial quantum number p is also an important quantum number but is much less investigated. LG modes with different p are orthogonal, which has potential applications in optical communications [11]. Recently, researchers developed p mode sorters of LG beams successfully with fractional Fourier transformation modules. These mode sorters can be applied in high-dimensional and multiphotonic quantum optical processes [12,13].

It is well known that the nonlinear optical process is a common way to realize frequency conversion. The phase mismatch affects the nonlinear conversion efficiency significantly. Birefringent phase matching [14,15] and quasiphase matching (QPM) [16,17] are the two widely used techniques to compensate for the phase mismatch. In recent years, nonlinear optical generation of vortex beams has attracted much attention [18,19]. Nonlinear process can be utilized to obtain a high frequency vortex beam source. Besides frequency and wave vector, in nonlinear processes of LG beams, conservation of two quantum numbers l and p is worthy of study. Azimuthal quantum number l has been demonstrated conservative in nonlinear optical process [20,21], and the radial quantum number p is found to be not conservative [20]. The output nonlinear beam is known to be a superposition mode, and the radial quantum number p of each component mode should be limited in a number range [22,23]. However, the propagation and conversion characteristics for individual component modes in the second-harmonic-generation (SHG) process are still unclear.

In this paper, deducing from the three-dimensional (3D) nonlinear paraxial equations, we have developed a nonlinear coupled equation set for the LG beam, which is able to describe the SHG process of LG beams more precisely, and the finite difference method is used to verify our results numerically. Furthermore, according to the coupled equation set, we can design a QPM crystal to manipulate the radial index of SH waves and obtain a LG beam with specific modes distribution.

II. RESULTS AND DISCUSSION

A. Analytic derivation of the selection rule

In this section, we deduce the nonlinear coupled equations of LG beam, with the similar method used to deduce the coupled equations of Gaussian beam [24,25].

*zhch@nju.edu.cn
†yqqin@nju.edu.cn

A pure linearly polarized LG beam propagating along the z axis is used as the input fundamental wave (FW). In general, we can use the nonlinear paraxial equation in a cylindrical coordinate system to describe the SHG process in a 1D optical superlattice (OSL):

$$\frac{\partial E_2(r, \varphi, z)}{\partial z} = -\frac{i}{2k_2}\nabla_T^2 E_2(r, \varphi, z)$$
$$-\frac{1}{2}iK_1E_1^2(r, \varphi, z)f(z)\exp(i\Delta kz), \quad (1)$$

where K_1 is the coupling coefficient. $f(z)$ is the structure function of the 1D OSL. k_1, k_2, E_1, E_2 are the wave vectors and electric fields for the FW and SH wave, respectively. $\Delta k = k_2 - 2k_1$ denotes the wave-vector mismatch. $\nabla_T^2 = \frac{\partial}{r\partial r}(\frac{r\partial}{\partial r}) + \frac{\partial^2}{r^2\partial\varphi^2}$ is the transverse Laplacian.

The expressions of LG modes can be written as

$$u_p^l(r, \varphi, z)$$
$$= \frac{A_p^l}{\omega(z)}\left[\frac{r\sqrt{2}}{\omega(z)}\right]^{|l|}\exp\left[\frac{-r^2}{\omega^2(z)}\right]L_p^{|l|}\left[\frac{2r^2}{\omega^2(z)}\right]$$
$$\times \exp\left[-\frac{ikr^2}{2R(z)} - il\varphi + (2p+l+1)\arctan\xi\right], \quad (2)$$

where l and p represent the azimuthal and radial index, respectively. $A_p^l = \sqrt{\frac{2p!}{\pi(p+|l|)!}}$ is the normalization constant. $\omega(z) = \omega_0\sqrt{1 + (\frac{z}{z_R})^2}$ is the beam waist at the position of z, with ω_0 denoting the beams waist at the focus. $z_R = \frac{k\omega_0^2}{2}$ is the Rayleigh range and k means the wave number. $L_p^{|l|}$ is the Laguerre polynomials. $R(z) = \frac{z_R^2+z^2}{z}$ is the radius of curvature of the wave front. $\xi = \frac{z}{z_R}$ is reducible propagation distance.

We choose $p = a$ mode as FW (hereafter we use p mode to refer to the LG mode with radial index p). ω_{01} is the beam waist of FW and Rayleigh range $z_R = \frac{k_1\omega_{01}^2}{2}$. We still use l to present the azimuthal index of FW, because the value of azimuthal index has been demonstrated to be conservative [20,21] and our derivation is universally valid for arbitrary value of azimuthal index. The expression of the fundamental wave is

$$E_1(r, \varphi, z) = B_1u_1(r, \varphi, z), \quad (3)$$

where B_1 is the amplitude of the $u_1(r, \varphi, z)$ and is constant in the condition of small signal approximation. The subscript represents the fundamental wave. $u_1(r, \varphi, z)$ is the expression

of $p = a$ mode and can be written as

$$u_1(r, \varphi, z) = \frac{A_a^l}{1 - i\xi}\left[\frac{\sqrt{2}r}{\omega_{01}\sqrt{1 + \xi^2}}\right]^{|l|}$$
$$\times \exp\left[\frac{-r^2}{\omega_{01}^2(1 - i\xi)}\right]L_a^{|l|}\left[\frac{2r^2}{\omega_{01}^2(1 + \xi^2)}\right]$$
$$\times \exp(-il\varphi)\exp[i(l + 2a)\arctan\xi]. \quad (4)$$

Because of the orthonormality of LG mode, we can use a series of LG modes as basis to expand the SH wave. The orthogonal LG mode should own same z and ω_0. Thus we choose the incident interface of crystal as the initial plane ($z = 0$) for both FW and SH wave. We choose $\omega_{02} = \sqrt{\frac{k_1}{k_2}}\omega_{01}$ to ensure that FW and SH wave have same z_R and ξ.

To research the compositions of SH wave, the expression of it can be written as

$$E_2(r, \varphi, z) = \sum_{n=0,1,2,\ldots} B_{2n}(z)u_{2n}(r, \varphi, z), \quad (5)$$

where the first subscript denotes the SH wave, and the second subscript n represents the mode of $p = n$ ($n = 0, 1, 2, \ldots$). $B_{2n}(z)$ is the expansion coefficient of $u_{2n}(r, \varphi, z)$, and also represents the amplitude of $p = n$ mode. $u_{2n}(r, \varphi, z)$ is the expression of $p = n$ mode and can be written as

$$u_{2n}(r, \varphi, z) = \frac{A_n^{2l}}{1 - i\xi}\left[\frac{\sqrt{2}r}{\omega_{02}\sqrt{1 + \xi^2}}\right]^{2|l|}$$
$$\times \exp\left[\frac{-r^2}{\omega_{02}^2(1 - i\xi)}\right]L_n^{2|l|}\left[\frac{2r^2}{\omega_{02}^2(1 + \xi^2)}\right]$$
$$\times \exp(-i2l\varphi)\exp[i(2l + 2n)\arctan\xi]. \quad (6)$$

Hereafter we omit the arguments r, φ and z in $u_1(r, \varphi, z)$, $u_{2n}(r, \varphi, z)$ and $B_{2n}(z)$ for convenience. Taking the slowly varying amplitude approximation and the paraxial approximation into consideration, it follows from Eq. (6) that

$$\nabla_T^2 u_{2n} - 2ik_2\frac{\partial u_{2n}}{\partial z} = 0. \quad (7)$$

Inserting Eqs. (3) and (5) into Eq. (1) and invoking Eq. (7), we obtain

$$\sum_{n=0,1,2,\ldots}\frac{dB_{2n}}{dz}u_{2n} = -\frac{1}{2}iK_1B_1^2u_1^2f(z)\exp(i\Delta kz). \quad (8)$$

Inserting Eqs. (4) and (6) into Eq. (8), we get

$$\sum_{n=0,1,2,\ldots}\frac{dB_{2n}}{dz}A_n^{2l}\exp(2ni\arctan\xi)L_n^{2|l|}\left[\frac{2r^2}{\omega_{02}^2(1 + \xi^2)}\right]$$

$$= -\frac{i}{2}K_1B_1^2(A_a^l)^2\frac{1}{1 - i\xi}\exp\left[\frac{r^2}{\omega_{02}^2(1 - i\xi)} - \frac{2r^2}{\omega_{01}^2(1 - i\xi)}\right]\left(\frac{\omega_{02}}{\omega_{01}}\right)^{2|l|}$$

$$\times \exp(4ai\arctan\xi)\left\{L_a^{|l|}\left[\frac{2r^2}{\omega_{01}^2(1 + \xi^2)}\right]\right\}^2 f(z)\exp(i\Delta kz). \quad (9)$$

The quadratic on the right-hand side can be expanded with a set of Laguerre Polynomials:

$$\left[L_a^{|l|}\left(\frac{k_1}{k_2}t\right)\right]^2 = \sum_{n=0}^{2a} C_n L_n^{2|l|}(t). \tag{10}$$

Here $t = \frac{2r^2}{\omega_{02}^2(1+\xi^2)}$, thus $\frac{k_1}{k_2}t = \frac{2r^2}{\omega_{01}^2(1+\xi^2)}$.

Inserting Eq. (10) into Eq. (9), we get

$$\sum_{n=0,1,2,\ldots} \frac{dB_{2n}}{dz} A_n^{2l} \exp{(2ni \arctan \xi)} L_n^{2|l|}(t)$$

$$= -\frac{i}{2} K_1 B_1^2 \left(A_a^l\right)^2 \frac{1}{1-i\xi} \exp\left[\left(\frac{k_2}{2k_1}-1\right)(1+i\xi)t\right] \left(\frac{k_1}{k_2}\right)^{|l|} \exp{(4ai \arctan \xi)} \left[\sum_{n=0}^{2a} C_n L_n^{2|l|}(t)\right] f(z) \exp{(i\Delta kz)}. \tag{11}$$

Here, if we suppose the phase mismatch is small, i.e., $\frac{k_2}{2k_1} - 1 \approx 0$ [23]. In order to insure that Eq. (11) is correct for all value of t, contrasting two sides of Eq. (11), we get

$$\frac{dB_{2n}}{dz} = -\frac{iK_1 B_1^2 \left(A_a^l\right)^2}{2^{l+1} A_n^{2l}} \frac{C_n}{1-i\xi} \exp{[(4a-2n)i \arctan \xi]} f(z) \exp{(i\Delta kz)}, \quad 0 \leqslant n \leqslant 2a,$$
$$B_{2n} = 0, \qquad\qquad\qquad n > 2a. \tag{12}$$

Mathematically, as mentioned in Ref. [23], a single p mode cannot constitute the SH wave, because the square of $L_a^{|l|}$ (Laguerre polynomial in the expression of FW) is not equal to every single Laguerre polynomial. After derivation, we demonstrate the component modes existing in SH wave should obey a special selection rule. A superposition mode composed of $2a + 1$ orthogonal modes ($p = 0, 1, 2, \ldots, 2a$) can constitute the SH, due to the Eq. (10). To conclude, for a FW with $p = a$, corresponding SH wave has $2a + 1$ modes ranged from $p = 0$ mode to $p = 2a$ mode, which is consistent with the experimental results in Ref. [22].

B. Propagation properties of the SH wave

Without loss of generality, we choose $p = 1$ mode as the FW to anaylse the propagation properties of SH wave. Eq. (12) can be rewrite as

$$\frac{dB_{20}}{dz} = C_0 \frac{\sqrt{(2l)!}}{2(l+1)!} iK_1' f(z) B_1^2 \frac{\exp{(i\Delta kz)}}{1-i\frac{z}{z_R}} \exp\left(4i \arctan \frac{z}{z_R}\right),$$

$$\frac{dB_{21}}{dz} = C_1 \frac{\sqrt{(2l+1)!}}{2(l+1)!} iK_1' f(z) B_1^2 \frac{\exp{(i\Delta kz)}}{1-i\frac{z}{z_R}} \exp\left(2i \arctan \frac{z}{z_R}\right), \tag{13}$$

$$\frac{dB_{22}}{dz} = C_2 \frac{\sqrt{(2l+2)!}}{2\sqrt{2}(l+1)!} iK_1' f(z) B_1^2 \frac{\exp{(i\Delta kz)}}{1-i\frac{z}{z_R}},$$

where $K_1' = \frac{\omega_{02}^{2l+2}}{\omega_{01}^{2l+1}} \sqrt{\frac{2}{\pi}} K_1$ is the modified coupling coefficient. Each cofficient can be figured out as

$$C_0 = (l+1)\left[(l+1) - \frac{2k_1}{k_2}(2l+1)\left(1 - \frac{k_1}{k_2}\right)\right],$$

$$C_1 = \frac{2k_1}{k_2}(l+1)\left(1 - \frac{2k_1}{k_2}\right),$$

$$C_2 = 2\left(\frac{k_1}{k_2}\right)^2. \tag{14}$$

Three modes constitute the SH wave as shown in Fig. 1, and their propagation properties can be described by Eq. (13). From Eq. (13), we find that three modes share most of propagation equations except additional phases appearing at the end of $p = 0$ and $p = 1$ mode's propagation equation. These additional phases are caused by the differences between Gouy phase shifts in each mode. Predictably, the propagation characteristics of each mode will dissimilate because of the impact of Gouy phase shifts.
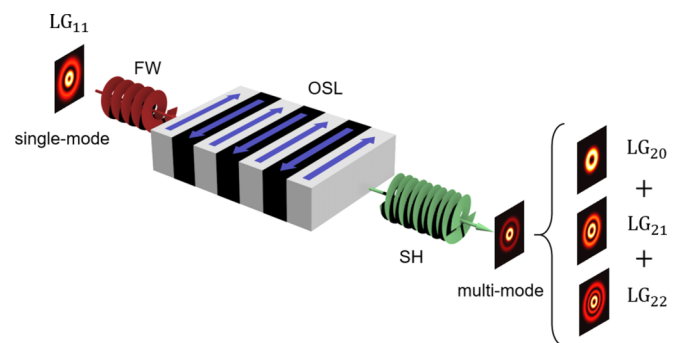

FIG. 1. Schematic diagram representing the second-harmonic generation of vortex beams in an optical superlattice.
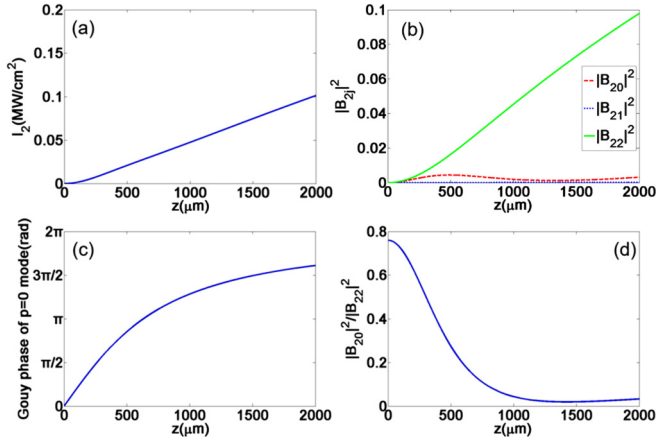
FIG. 2. Simulation of the dependence of (a) SH intensity, (b) the modular square of amplitude, (c) specific value and (d) the Gouy phase of $p = 0$ mode on propagation distance z ranged from $z = 0$ to $z = 2000\,\mu$m.

The coupled equation set Eq. (13) can describe the propagation properties of each component mode in the SH wave accurately. By solving Eq. (13) numerically, we obtain the amplitudes B_{2j} ($j = 0, 1, 2$). Inserting B_{2j} and the expression of LG mode u_{2j} into Eq. (3), we can numerical calculate and illustrate the phase and intensity profiles of SH. In previous work such as Ref. [20], the SH wave of the LG beam is usually studied as a whole. However, in our method the SH wave is considered as a superposition mode and each mode in the SH wave can be studied separately. Thus we named it the superposition mode method.

The propagation of each mode in SH wave is simulated on the basis of the Eq. (13). We use LG_{11} mode at the wavelength (λ) of 1064 nm as FW, which propagates along z axis and has a beam waist (ω_0) of 10 μm. We use a periodically poled lithium tantalate to induce SHG. The coherence length l_c is 3.92 μm at 25 °C, while FW and SH wave share the same Rayleigh range $z_R = 631.98\,\mu$m. The period of the crystal is $2l_c$, while the reciprocal lattice vector can compensate for phase mismatch. The area we considered is 100 μm × 100 μm composed of 400 × 400 grids. It is well-known that l is conserved in the SHG process, thus we mainly research the properties of radial quantum number p and ignore the azimuthal quantum number l. Figure 2(a) shows the dependence of the intensity of SH wave on propagation distance z ranged from $z = 0$ to $z = 2000\,\mu$m · I_2 has an expected quadratic rise at the beginning of the propagation, but the Gouy phase shift causes an accumulated phase shift and affects I_2 in the long distance. Figure 2(b) shows the dependence of the modular square of amplitude $|B_{2j}|^2$ on the propagation distance z. Because of the orthonormality of LG mode, $|B_{2j}|^2$ represents the intensity of each component in SH. This figure shows that $p = 0$ and $p = 2$ are two main modes in the SH wave, because C_1 is close to 0. The solid green line representing $|B_{22}|^2$ increases monotonically, while the dashed red line representing $|B_{20}|^2$ continues to rise after one oscillation, because the existence of a Gouy phase shift affects the QPM condition and reduces conversion efficiency, just as occurs in Gaussian beams [20,21]. More specifically, the value of the
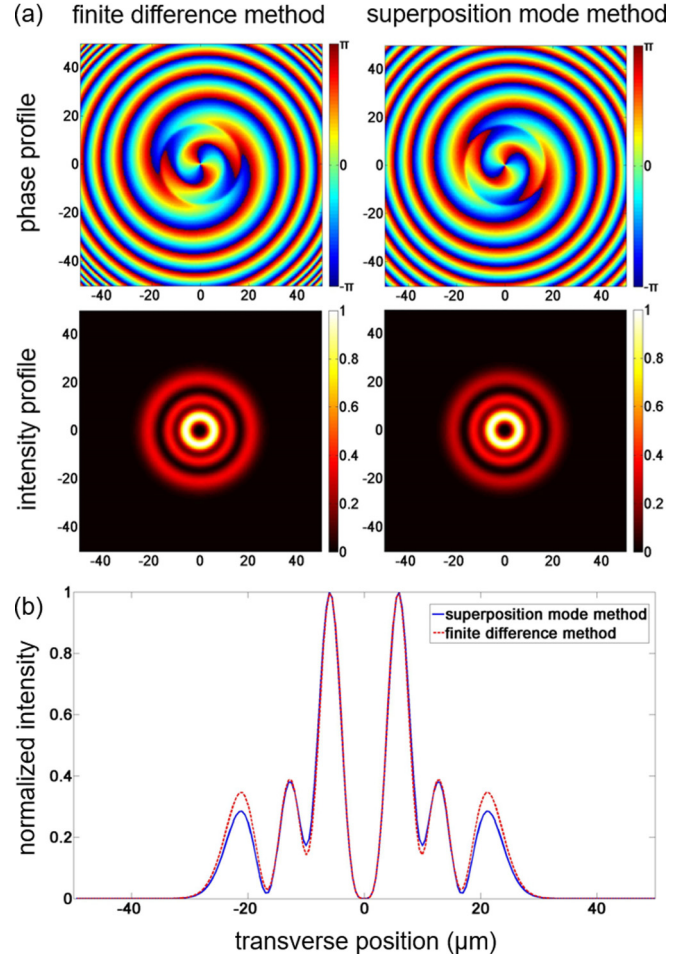

FIG. 3. (a) Phase and amplitude profile, (b) intensity distribution at center line of SH wave with different methods at 600 μm. Two sets of intensity profiles and curves are nearly identical, and the correlation coefficient R is 0.9939.

Gouy phase in $p = 0$ mode varies from 0 to π while the FW propagates from 0 to z_R in crystal, and approaches 2π with propagation at last. As shown in Fig. 2(c), the additional phase π will induce equivalent domain inversion and break the QPM condition in $p = 0$ mode around Rayleigh range, as a result, the intensity of $p = 0$ mode declines from about 500 to 1200 μm. In contrast, the $p = 2$ mode satisfies the QPM condition through the whole SHG process and its intensity will increase monotones. Furthermore, we can design an OSL with a particular length to produce desired SH multimode on the basis of the relation between propagation distance and intensity of each mode. The ratio of two main modes' intensity decreases from 0.7597 to 0.0196 as shown in Fig. 2(d). Thus we can produce a superposition two-mode SH wave with arbitrary ratio during this range.

We next simulate the normalized intensity and phase profile of SH wave by the superposition mode method. We select three sets of data at the propagation distance of 200, 600, and 1000 μm. The results of 600 μm are shown in Fig. 3. To check our theory, we also use the finite difference method to simulate the distribution of SH wave [26]. This method is a common and effective way to calculate nonlinear optical processes. The influence of backflow of FW is considered by this method.
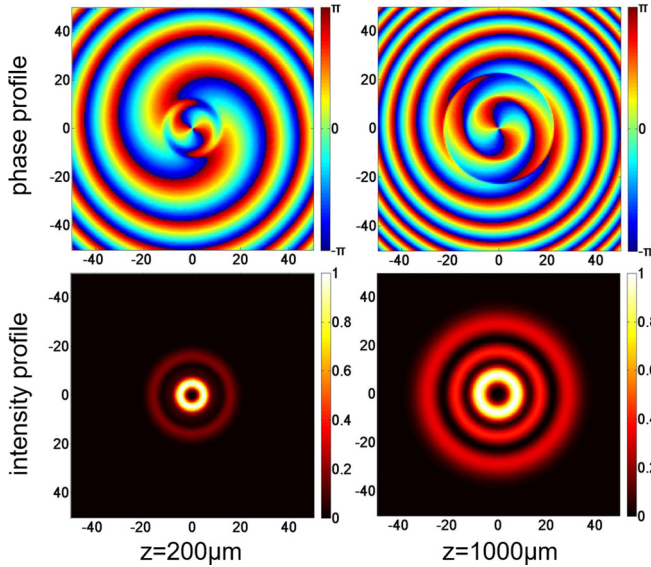
FIG. 4. Phase and amplitude profile at 200 and 1000 μm. In the intensity profile at $z = 200\,\mu$m, the inner ring is much brighter than outer ring, because both $p = 0$ and $p = 2$ mode have large proportion in the SH wave, while at $z = 1000\,\mu$m the proportion of $p = 2$ mode is much larger than other ones.

The two series of profiles are almost identical as shown in Fig. 3(a). We still analyze the intensity distribution at the center line. Two curves almost coincide as shown in Fig. 3(b). To compare the results between the two methods precisely, we introduce the correlation coefficient R. I_1 and I_2 represent the SH intensity (simulated) calculated from the finite difference method and superposition mode method, respectively. Then the correlation coefficient R can be expressed as

$$R = \frac{n\sum_{i=1}^{n} I_{1i}I_{2i} - \sum_{i=1}^{n} I_{1i}\sum_{i=1}^{n} I_{2i}}{\sqrt{n\sum_{i=1}^{n} I_{1i}^2 - \left(\sum_{i=1}^{n} I_{1i}\right)^2}\sqrt{n\sum_{i=1}^{n} I_{2i}^2 - \left(\sum_{i=1}^{n} I_{2i}\right)^2}}. \tag{15}$$

The correlation coefficient represents the degree of similarity between two physical quantities. The closer the correlation coefficient is to 1, the higher the degree of similarity between the two physical quantities will be. After calculation, we get $R = 0.9955$ at 200 μm, $R = 0.9939$ at 600 μm and $R = 0.9956$ at 1000 μm. These results give strong support to our calculation and theory. Moreover, in the case of phase matching, our theory is entirely accurate and we get $R = 1$ at all propagation distances.

C. The production of a controllable multimode vortex beam source

In the last section, we demonstrated that the propagation distance in crystal impacts the energy distribution in the SH wave. In other words, we can modulate the ratio of the two main modes' intensity by controlling the length of the crystal. The ratio ranges from 0.0196 to 0.7597 as shown in Fig. 2(d). In this section, we compare the normalized intensity and phase profile of the SH wave at 200 and 1000 μm. As shown in Fig. 4, in the phase profiles, the number of 2π cycles around the circumference is the azimuthal quantum number l. It is
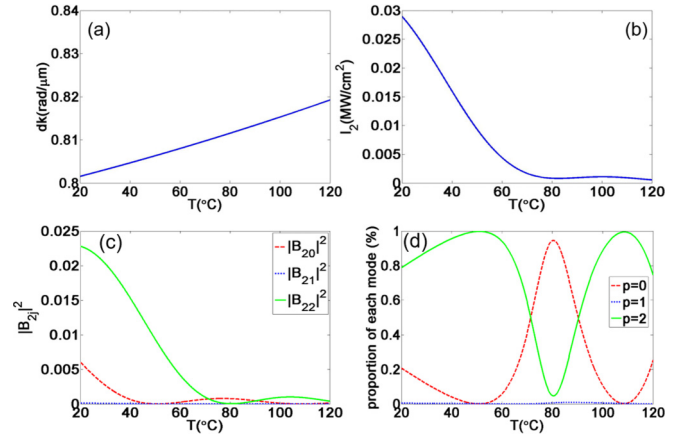

FIG. 5. Simulation of the dependence of (a) phase mismatch, (b) intensity of SH wave, (c) the modular square of amplitude and (d) proportion of each mode on crystal temperature T from $T = 20\,°$C to $T = 120\,°$C.

obvious that the azimuthal quantum number l of SH is 2, which strictly obeys the conservation of OAM. In general, the number of the radial saltation is the radial quantum number p. However, the radial saltation warps in this case. The phase profile of SH is mainly a weighted sum of $p = 0$ and $p = 2$ modes. In the intensity profiles, a central dark hole exists because of the phase singularity. The number of dark rings between two bright rings is related to the radial quantum number p. It is equal to p in a pure LG mode's intensity profile, but cannot reflect actual situation in a superposition mode. In the intensity profile at $z = 200\,\mu$m, the inner ring is much brighter than the outer ring, because both $p = 0$ and $p = 2$ mode have large proportion in the SH wave [$\frac{|B_{20}|^2}{|B_{22}|^2} = 0.6268$ as shown in Fig. 2(b)]. In the case of $z = 1000\,\mu$m, the intensity profile looks like the profile of a pure $p = 2$ mode, because $|B_{20}|^2$ is much smaller than $|B_{22}|^2$ ($\frac{|B_{20}|^2}{|B_{22}|^2} = 0.0436$).

Besides the length of crystal, other physical quantities, such as temperature, have an impact on the SH wave as well, and can also be used in mode modulation. It is worth mentioning that changing the length of the crystal is a direct method, but is difficult to achieve in experiment. Sorting the beam by controlling the temperature (T) of the crystal is more realizable in experiment. We adjust temperature to change the refractive index, further to change phase mismatch and oscillating period. A deviation between corresponding oscillating periods will also appear because of the different Gouy phase shifts. Besides the phase mismatch, the temperature also influences modified coupling coefficient K_1' and coefficients C_j. Thus the evolution of each mode in the SH will be too complicated to analytically calculate. We next stimulate the dependence of the modular square of amplitude on a temperature ranging from 20 to 120 °C. We set the beam waist and crystal length to $\omega_0 = 10\,\mu$m and $z = 600\,\mu$m and use the same QPM crystal as the one in last section, which achieves QPM at $T = 25\,°$C. The change of temperature influences the phase mismatch directly, and their relationship is shown in Fig. 5(a). Figure 5(b) shows the dependence of SH intensity on temperature. The change of temperature breaks the QPM, thus the nonlinear conversion efficiency goes down. Intensity

and proportion of each mode are shown in Figs. 5(c) and 5(d), respectively. Under our simulations, the proportion of $p = 0$ mode is ranged from 0.02% at $T = 50.9\,°C$ to 94.56% at $T = 80.4\,°C$, while the proportion of $p = 2$ mode is ranged from 4.74% at $T = 80.5\,°C$ to 99.80% at $T = 51.0\,°C$. The $p = 1$ mode is just the minority with a proportion of no more than 0.00169%. From our simulation, we successfully modulate the multimode SH wave by changing temperature and the adjustable ranges of the proportion of two main modes are large enough.

All of the above is perfectly compatible with our calculation. It is proved that high frequency vortex beams generated by nonlinear process is multicomponent and impure. This feature may provide potential applications. The intensity of the main modes in the SH wave can be modulated. By analyzing the coupled equation set for LG beams, we know the propagation characteristics of each mode in the SH wave. By changing the length, temperature or other features of structure, we can precisely control the energy distribution in the SH wave. It means we can design a crystal that is controllable, and can convert a single-mode vortex beam into a multimode one, and simultaneously implement frequency doubling and p mode expansion. The application of p mode multiplexing in optical communication is limited, because only the beams from the same source, which have same propagation distance all the time, are mutually orthogonal. Modes emitted from our crystal exactly satisfy this condition. Thus the designed crystal has potential applications in mode division multiplexing system.

D. Discussion

Our analysis can be generalized to other nonlinear process, such as sum-frequency generation and third-harmonic generation. A higher order p mode or superposition mode can also be used as FW, and the situation will be more complex and deserves future investigation. In our discussion, the input wave is a linearly polarized wave, thus we can use the scalar nonlinear paraxial equation to study the conversion and propagation of the LG beam. It should be noted that the scalar equation is not applicable to the case of circular polarized waves, where the conservation of circular polarization should be taken into consideration. Furthermore, the nonconservation of radial index p in the nonlinear process can be compared with the nonconservation of wave vector k. The nonconservation of the wave vector, i.e., the phase mismatch, limits the nonlinear conversion efficiency, and how to compensate this mismatch is an unavoidable problem in every nonlinear optical process. On the contrary, the nonconservation of the radial index causes the mixture of different modes, instead of limiting the nonlinear conversion efficiency, and shows the potential applications in optical communication. Obviously, the physical properties of these two quantum numbers have clear distinctions. With the further research, we believe the physical meaning of radial index will be ascertained.

It is also worth discussing the validity of the paraxial approximation in the SHG process involving LG beams. In 2007, Vaveliuk *et al.* proposed an efficient paraxiality estimator P to evaluate the validity of paraxial approximation [27], which can be expressed as

$$P = 1 - \frac{2p + |l| + 1}{(k\omega_0)^2}. \tag{16}$$

The closer the efficient paraxiality estimator is to 1, the more valid the paraxial approximation will be. In our case, the paraxiality estimators of the FW and each SH component are found to be $P_1 = 0.9997$, $P_{20} = 0.9998$, $P_{21} = 0.9997$, and $P_{22} = 0.9996$, respectively. Thus, we consider that the influence of paraxial approximation is quite acceptable.

III. CONCLUSION

To conclude, we clarify the conservation problem of radial quantum number in the SHG process of LG beams with the paraxial approximation. We verify that the SH wave is in a superposition mode, and the component modes obey a selection rule, which agrees with former research. We derive the coupled equation set for LG beams to describe the propagation properties of the SHG. Under the guidance of our equations, we can modulate each component mode wave separately, instead of treating the SH wave as a whole. Furthermore, we show that a periodical QPM crystal can be used to produce a multimode SH vortex beam. By changing the length and temperature of the crystal, we can manipulate each mode and realize mode division multiplexing.

ACKNOWLEDGMENTS

---

[1] M. W. Beijersbergen, R. J. C. Spreeuw, L. Allen, and J. P. Woerdman, Multiphoton resonances and Bloch-Siegert shifts observed in a classical two-level system, Phys. Rev. A **45**, 1810 (1992).

[2] J. Ng, Z. Lin, and C. T. Chan, Theory of Optical Trapping by an Optical Vortex Beam, Phys. Rev. Lett. **104**, 103601 (2010).

[3] S. Mei, K. Huang, T. Zhang, M. Q. Mehmood, H. Liu, C. T. Lim, J. Teng, and C.-W. Qiu, Evanescent vortex: Optical subwavelength spanner, Appl. Phys. Lett. **109**, 191107 (2016).

[4] H. Huang, Guodong Xie, Yan Yan, Nisar Ahmed, Yongxiong Ren, Yang Yue, Dvora Rogawski, Moshe J. Willner, Baris I. Erkmen, Kevin M. Birnbaum *et al.*, 100 Tbit/s free-space data link enabled by three-dimensional multiplexing of orbital angular momentum, polarization, and wavelength, Opt. Lett. **39**, 197 (2014).

[5] A. Mair, A. Vaziri, G. Weihs, and A. Zeilinger, Entanglement of the orbital angular momentum states of photons, Nature **412**, 313 (2001).

[6] A. Vaziri, G. Weihs, and A. Zeilinger, Experimental Two-Photon, Three-Dimensional Entanglement for Quantum Communication, Phys. Rev. Lett. **89**, 240401 (2002).

[7] K. A. Forbes and D. L. Andrews. Optical orbital angular momentum: Twisted light and chirality, Opt. Lett. **43**, 435 (2018).

[8] W. Brullot, M. K. Vanbel, T. Swusten, and T. Verbiest, Resolving enantiomers using the optical angular momentum of twisted light, Sci. Adv. **2**, e1501349 (2016).

[9] L. Rego, K. M. Dorney, N. J. Brooks, Q. Nguyen, C-T. Liao, J. S. Román, D. E. Couch, A. Liu, E. Pisanty, M. Lewenstein, L. Plaja, H. C. Kapteyn, M. M. Murnane, and C. Hernández-García, Light with a self-torque: Extreme-ultraviolet beams with time-varying orbital angular momentum, Science **364**, eaaw9486 (2019).

[10] W. N. Plick and M. Krenn, Physical meaning of the radial index of Laguerre-Gauss beams, Phys. Rev A **92**, 063841 (2015).

[11] V. D. Salakhutdinov, E. R. Eliel, and W. Löffler, Full-Field Quantum Correlations of Spatially Entangled Photons, Phys. Rev. Lett. **108**, 173604 (2012).

[12] Y. Zhou, M. Mirhosseini, D. Fu, J. Zhao, S. M. Hashemi Rafsanjani, A. E. Willner, and R. W. Boyd, Sorting Photons by Radial Quantum Number, Phys. Rev. Lett. **119**, 263602 (2017).

[13] X. Gu, M. Krenn, M. Erhard, and A. Zeilinger, Gouy Phase Radial Mode Sorter for Light Concepts and Experiments, Phys. Rev. Lett. **120**, 103601 (2018).

[14] L. Golovan, V. Y. Timoshenko, A. Fedotov, L. Kuznetsova, D. Sidorov Biryukov, P. Kashkarov, A. Zheltikov, D. Kovalev, N. Kunzner, and E. Gross, Phase matching of second-harmonic generation in birefringent porous silicon, Appl. Phys. B **73**, 31 (2001).

[15] N. Dong, F Chen, and J. Vazquez de Aldana, Efficient second harmonic generation by birefringent phase matching in femtosecond-laser-inscribed KTP cladding waveguides, Phys. Status SolidiRRL **6**, 306 (2012).

[16] M. M. Fejer, G. A. Magel, D. H. Jundt, and R. L. Byer, Quasi-phase-matched second harmonic generation: Tuning and tolerancesIEEE J. Quantum Electron. **28**, 2631 (1992).

[17] Y.-Q. Lu, Y.-Y. Zhu, Y.-F. Chen, S.-N. Zhu, N.-B. Ming, and Y.-J. Feng, Optical properties of an ionic-type phononic crystal, Science **284**, 1822 (1999).

[18] X.-F. Ren, G.-P. Guo, B. Yu, J. Li, and G.-C. Guo, The orbital angular momentum of down-converted photons, J. Opt. B **6**, 243 (2004).

[19] K. Shemer, N. Voloch-Bloch, A. Shapira, A. Libster, I. Juwiler, and A. Arie, Azimuthal and radial shaping of vortex beams generated in twisted nonlinear photonic crystals, Opt. Lett. **38**, 5470 (2013).

[20] G.-h. Shao, Z.-j. Wu, J.-h. Chen, F. Xu, and Y.-q. Lu, Nonlinear frequency conversion of fields with orbital angular momentum using quasiphase-matching, Phys. Rev. A **88**, 063827 (2013).

[21] Z.-Y. Zhou, D.-S. Ding, Y.-K. Jiang, Y. Li, S. Shi, X.-S. Wang, and B.-S. Shi, Orbital angular momentum light frequency conversion and interference with quasiphase matching crystals, Opt. Express **22**, 20298 (2014).

[22] J. Courtial, K. Dholakia, L. Allen, and M. J. Padgett, Second-harmonic generation and the conservation of orbital angular momentum with high-order Laguerre-Gaussian modes, Phys. Rev. A **56**, 4193. (1997).

[23] L. D. Romero, D. L. Andrews, and M. Babiker, A quantum electrodynamics framework for the nonlinear optics of twisted beams, J. Opt. B **4**, S66. (2002).

[24] G.-D. Xu, T.-W. Ren, Y.-H. Wang, Y.-Y. Zhu, S.-N. Zhu, and N.-B. Ming, Third-harmonic generation by use of focused Gaussian beams in an optical superlattice, J. Opt. Soc. Am. B **20**, 360 (2003).

[25] C. Zhang, Y.-q. Qin, and Y.-y. Zhu, Perfect quasiphase matching for the third harmonic generation using focused Gaussian beams, Opt. Lett. **33**, 720 (2008).

[26] M.-s. Zhou, J.-c. Ma, C. Zhang, and Y.-q. Qin, Numerical simulation of nonlinear field distribution in two-dimensional optical superlattice, Opt. Express **20**, 1261 (2012).

[27] P. Vaveliuk, B. Ruiz, and A. Lencina, Limits of the paraxial approximation in laser beams, Opt. Lett. **32**, 927 (2007).